

# Disentanglement via Latent Quantization

Kyle Hsu<sup>†</sup> Will Dorrell<sup>‡</sup> James C. R. Whittington<sup>†§</sup> Jiajun Wu<sup>†</sup> Chelsea Finn<sup>†</sup>  
<sup>†</sup>Stanford University <sup>‡</sup>University College London <sup>§</sup>Oxford University  
 {kylehsu, jiajunwu, cbfinn}@cs.stanford.edu {dorrellwec, jcrwhittington}@gmail.com

## Abstract

In disentangled representation learning, a model is asked to tease apart a dataset’s underlying sources of variation and represent them independently of one another. Since the model is provided with no ground truth information about these sources, inductive biases take a paramount role in enabling disentanglement. In this work, we construct an inductive bias towards compositionally encoding and decoding data by enforcing a harsh communication bottleneck. Concretely, we do this by (i) quantizing the latent space into learnable discrete codes with a separate scalar codebook per dimension and (ii) applying strong model regularization via an unusually high weight decay. Intuitively, the quantization forces the encoder to use a small number of latent values across many datapoints, which in turn enables the decoder to assign a consistent meaning to each value. Regularization then serves to drive the model towards this parsimonious strategy. We demonstrate the broad applicability of this approach by adding it to both basic data-reconstructing (vanilla autoencoder) and latent-reconstructing (InfoGAN) generative models. In order to reliably assess these models, we also propose InfoMEC, new metrics for disentanglement that are cohesively grounded in information theory and fix well-established shortcomings in previous metrics. Together with regularization, latent quantization dramatically improves the modularity and explicitness of learned representations on a representative suite of benchmark datasets. In particular, our quantized-latent autoencoder (QLAE) consistently outperforms strong methods from prior work in these key disentanglement properties without compromising data reconstruction.

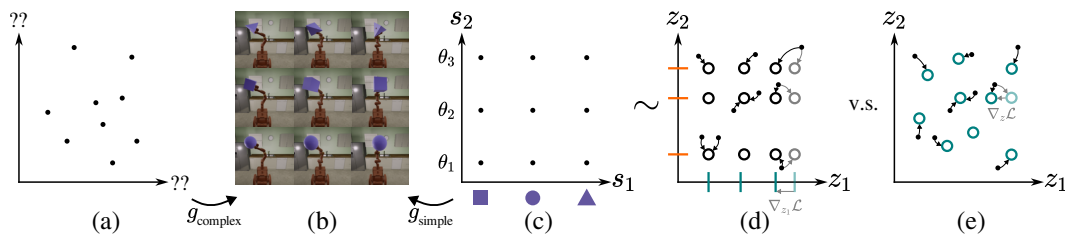


Figure 1: Motivating observations and overview of the inductive bias of latent quantization. The mapping between true sources (c) and data (b) is simpler than most other possible generative functions from unstructured domains (a). To help recover the sources, we use quantized latents (d)—continuous latents (dots) are mapped (via arrows) to their nearest discrete codes (black circles), each of which is constructed combinatorially from per-dimension scalar codebooks (turquoise and orange ticks). In contrast, vector quantization (e) [51] individually represents vector embeddings (turquoise circles). A compositional inductive bias manifests in how the codes change from previous values (grayed): the combinatorially defined codes move in lockstep and change the quantization of many latents, whereas the individual embeddings move separately and have a comparatively local effect.

# 1 Introduction

Our increasing reliance on black-box methods for processing high-dimensional data underscores the importance of developing techniques for learning human-interpretable representations. To name but a few possible benefits, such representations could foster more informed human decision-making [56, 26], facilitate efficient model debugging and improvement [16, 40], and streamline auditing and regulation [47, 14]. In this context, disentangled representation learning serves as a worthwhile scaffolding: loosely speaking, its goal is for a model to tease apart a dataset’s underlying sources of variation and represent them independently of one another.

Accomplishing this, however, has proven difficult. Conceptually, the field lacks a formal problem statement that resolves fundamental ambiguities [29, 42] without overly restrictive assumptions (reviewed in Section 6); methodologically, evaluation metrics have been found to be uncalibrated, sensitive to hyperparameters, or sample inefficient [10]; and empirically, there is still a need for an inductive bias that enables consistently good performance in the purely unsupervised setting.

In this work, we answer the call for a better inductive bias for disentanglement. Our solution is motivated by observing that many datasets of interest are generated from their sources in a compositional manner (Figure 1). This distinguishing property of realistic generative processes applies to real world physics as well as human approximations thereof (e.g., rendering). Hence, our broad strategy to uncover the true underlying sources is to bias the model towards compositionally encoding to and decoding from its latent space.

We manifest this inductive bias by drawing from two common ideas in the machine learning literature: discrete representations [51] and model regularization. Specifically, we propose (i) quantizing a model’s latent representation into learnable discrete values with a separate scalar codebook per dimension and (ii) applying strong regularization via an unusually high weight decay [44]. Intuitively, forcing the model to reuse a small number of values that combinatorially construct the latent code encourages it to assign a consistent meaning to each value, an outcome that weight decay explicitly incentivizes by regularizing towards parsimony.

A side benefit of models with quantized latents is that they sidestep one issue that has hindered evaluation in previous works: they enable the use of simpler, more robust distribution estimation techniques. As a further methodological contribution, we present InfoMEC, new metrics for the modularity, explicitness, and compactness of disentangled representations that are cohesively grounded in information theory and fix other well-established shortcomings in existing metrics.

We demonstrate the broad applicability of latent quantization by adding it to both basic data-reconstructing (vanilla autoencoder) and latent-reconstructing (InfoGAN) generative models. Together with regularization, this is sufficient to dramatically improve the modularity and explicitness of the learned representations. On a representative suite of four disentangled representation learning datasets with image observations and ground-truth source evaluations [9, 19, 49], our quantized-latent autoencoder (QLAE, pronounced like clay) consistently outperforms strong methods from prior work without compromising data reconstruction.<sup>1</sup> We think of QLAE as exemplifying a minimalist specification of a compositional inductive bias in neural networks, suggesting that our recipe of latent quantization and regularization could be broadly useful to other areas of machine learning.

## 2 Preliminaries

In order to properly contextualize our proposed inductive bias, methodological contributions, and experiments, we first devote some attention to explaining the problem of disentangled representation learning. We also discuss prior disentangled representation learning methods we build upon.

### 2.1 Nonlinear ICA and Disentangled Representation Learning

We begin by considering the standard data-generating model of nonlinear independent components analysis (ICA) [29], a very related but more conceptually precise problem than disentanglement:

$$p(\mathbf{s}) = \prod_{i=1}^{n_s} p(\mathbf{s}_i), \quad \mathbf{x} = g(\mathbf{s}), \tag{1}$$

---

<sup>1</sup>We provide a modular code repository implementing all methods considered in this work as well as InfoMEC estimation at <https://github.com/kylehksu/disentangle>.

where  $\mathbf{s} = (\mathbf{s}_1, \dots, \mathbf{s}_{n_s})$  comprise the  $n_s$  mutually independent source variables (sources);  $\mathbf{x}$  is the observed data variable; and  $g : \mathcal{S} \rightarrow \mathcal{X}$  is the nonlinear data-generating function. The nonlinear ICA problem is to recover the underlying sources given a dataset  $\mathcal{D}$  of samples from this model. Specifically, the solution should include an approximate inverting function  $\hat{g}^{-1} : \mathcal{X} \rightarrow \mathcal{Z}$  such that, assuming latent variables (latents)  $\mathbf{z} = (\mathbf{z}_1, \dots, \mathbf{z}_{n_s})$  are matched correctly to the sources, each source is perfectly determined by its corresponding latent. A typical technical phrasing is that  $\hat{g}^{-1} \circ g$  should be the composition of a permutation and a dimension-wise invertible function.

As stated, this problem is *nonidentifiable* (or underspecified). Given  $\mathcal{D}$ , one may find many sets of independent latents (and associated nonlinear generators) that fit the data but are non-trivially different from the true generative sources [29]. As such, reliably recovering the true sources from the data is impossible. Much recent work in nonlinear ICA has focused on proposing additional problem assumptions so as to provably pare down the possibilities to a unique solution. These theoretical assumptions can then be transcribed into architectural choices in a learned model or regularization terms in the optimization objective. Such approaches have shown promise in increasing our understanding of what assumptions are required to disentangle; we elaborate on this in Section 6.

While identifiability is conceptually appealing, achieving it under sufficiently generalizable assumptions that apply to non-toy datasets has proven hard. The field of disentangled representation learning has taken a more pragmatic approach, focusing on empirically evaluating the recovery of each dataset’s designated source set. Given this empirical focus, robust performance metrics are vital. Unfortunately, there is a plethora of approaches in use, and subtle yet impactful issues arise even in the most common choices [10]. To address these concerns, in Section 4 we propose new metrics for three existing, complementary notions of disentanglement [17, 54]. They measure the following three properties: **modularity**—the extent to which each source is encoded in disjoint sets of latents; **explicitness**—how *simply* the latents encode each source; and **compactness**—the extent to which each latent contains information about disjoint sets of sources. We frame these three in a cohesive information-theoretic framework that we call InfoMEC.

The disentangled representation learning problem statement considered in this work is as follows. Given a dataset of paired source-data samples  $\{(s, x = g(s))\}$  from the nonlinear ICA model (1), learn an encoder  $\hat{g}^{-1} : \mathcal{X} \rightarrow \mathcal{Z}$  and decoder  $\hat{g} : \mathcal{Z} \rightarrow \mathcal{X}$  solely using the data  $\{x\}$  such that (i) the InfoMEC as estimated from samples  $\{(s, z = \hat{g}^{-1} \circ g(s))\}$  from the joint source-latent distribution is high, while (ii) maintaining an acceptable level of reconstruction error between  $x$  and  $\hat{g} \circ \hat{g}^{-1}(x)$ .

## 2.2 Autoencoding and InfoGAN as Data and Latent Reconstruction

We will apply our proposed latent quantization scheme to two foundational approaches for disentangled representation learning: vanilla autoencoders (AEs) and information-maximizing generative adversarial networks (InfoGANs) [12]. Here, we provide a brief overview linking the two as reconstructing data and latents, respectively, and defer complete implementation details to Appendices A and B. Both approaches involve learning an encoder  $\hat{g}^{-1}$  and decoder  $\hat{g}$ . An autoencoder takes a datapoint  $x \in \mathcal{X}$  as input and produces a reconstruction  $\hat{g} \circ \hat{g}^{-1}(x) \in \mathcal{X}$  that is optimized to match the input:

$$\mathcal{L}_{\text{reconstruct data}}(\hat{g}^{-1}, \hat{g}; \mathcal{D}) := \mathbb{E}_{x \sim \mathcal{D}} [-\log p(x | \hat{g} \circ \hat{g}^{-1}(x))]. \quad (2)$$

An InfoGAN instead takes a latent code  $z \in \mathcal{Z}$  as input. The decoder (aka generator) maps  $z$  to the data space, and from this the encoder produces a reconstruction of the latent:

$$\mathcal{L}_{\text{reconstruct latent}}(\hat{g}^{-1}, \hat{g}) := \mathbb{E}_{z \sim p(z)} [-\log p(z | \hat{g}^{-1} \circ \hat{g}(z))]. \quad (3)$$

Unlike the data reconstruction loss, this is clearly insufficient for learning as the dataset  $\mathcal{D}$  isn’t even used. InfoGAN can be thought of as grounding latent reconstruction by making the marginal distribution of generated datapoints,  $\hat{g}(z)$ , indistinguishable from the empirical data distribution. A concrete measure of this is provided by an additional binary classifier (aka discriminator) [20] or value model (aka critic) [1] trained alongside but in opposition to the decoder. While InfoGAN was originally motivated as maximizing a variational lower bound on the mutual information between the latent and the generated data, we find the above interpretation to be unifying.

## 3 Latent Quantization

As mentioned in Section 1, we want to encourage our model to disentangle by biasing it towards using a compositional latent space. Why would this mitigate the nonidentifiability of nonlinear ICA? While

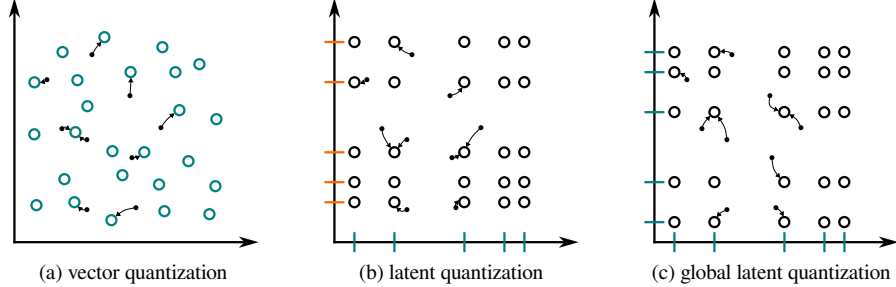


Figure 2: (a) Vector quantization maps continuous latents (black dots) to their nearest codes (circles); each code’s position is optimized separately over the course of training. (b) Latent quantization maps latents onto a regularly-structured grid in which only the per-dimension codebooks (orange and turquoise ticks) are optimized. (c) We also tested global latent quantization, in which every dimension shares the same codebook. In this schematic, each strategy has 25 codes, but defines them using either (a) 50, (b) 10, or (c) 5 parameters.

currently we can only support this with empirical evidence, our key motivation is that generative models for realistic data are compositional, and this should be appropriately reflected in the model.

To build this inductive bias, we propose latent quantization, a modification of vector quantization [51]. In the latter, the latent representation of a datapoint is partitioned into component vectors, each of which is quantized to the nearest of a discrete set of vector embeddings (Figure 2a). We modify vector quantization to enforce a harsh communication bottleneck that can be circumvented by encoding and decoding compositionally. Specifically, we propose that the set of latent codes should be the Cartesian product of  $n_z$  distinct scalar codebooks:  $Z = V_1 \times \dots \times V_{n_z}$ , where each codebook,  $V_j$ , is a set of  $n_v$  reals. The complete transformation comprises, first, the encoder network mapping the data to a continuous latent space  $\hat{g}^{-1} : \mathcal{X} \rightarrow \mathbb{R}^{n_z}$  (with a slight abuse of notation), followed by quantization onto the nearest code (Figure 2b). A side advantage of this scheme is that the nearest neighbor calculation can be done elementwise, which is highly efficient. (This is the motivation others have used to arrive at similar methods [3, 61, 30, 66].) Formally, latent quantization is:

$$z_j = \arg \min_{v_{jk}} |\hat{g}^{-1}(x)_j - v_{jk}|, \quad v_{jk} \in V_j, \quad j = 1, \dots, n_z. \quad (4)$$

We represent  $Z$  by its constituent discrete values, concretely as a learnable two-dimensional array  $V \in \mathbb{R}^{n_z \times n_v}$ , the  $j$ -th row of which stores the elements of codebook  $V_j$  in an arbitrary order.

A lesson from nonlinear ICA is that, given a flexible enough model, data can be mapped to and from structured latent spaces in many meaningless ways, circumventing the hopes of their designers. We motivate the use of strong model regularization with the conjecture that, of all the theoretically possible mappings from compositional latent space to data, the most parsimonious will be the true generative model or something close enough to it. We operationalize this by using a high weight decay on both the encoder and decoder networks. Ablation studies (Section 5) show that both compositional quantized latents and weight decay are necessary to disentangle well.

To train a quantized-latent model, we co-opt the straight-through gradient estimator [5] as well as the quantization and commitment losses proposed for vector quantization:

$$\mathcal{L}_{\text{quantize}} = \|\text{StopGradient}(\hat{g}^{-1}(x)) - z\|_2^2, \quad \mathcal{L}_{\text{commit}} = \|\hat{g}^{-1}(x) - \text{StopGradient}(z)\|_2^2. \quad (5)$$

The straight-through gradient estimator facilitates the flow of gradients through the nondifferentiable quantization step.  $\mathcal{L}_{\text{quantize}}$  pulls the discrete values constituting  $z$  onesidedly towards the pre-quantized continuous output of the encoder. This is needed to optimize  $V$ , since straight-through gradient estimation disconnects  $V$  from the computation graph. Conversely, the commitment loss prevents the pre-quantized representation, which does see gradients from downstream computation, from straying too far from the codes. While this is a significant failure mode for vector quantization, we find that using scalar codebooks instead of high-dimensional embedding vectors alleviates this issue, allowing us to drastically downweight the quantization and commitment losses while maintaining training stability. This gives the model much-needed flexibility to reorganize the discrete latent space. Finally, while using a shared global scalar codebook would result in an even stricter bottleneck (Figure 2c), we find it slightly better to maintain separate codebooks for the

sake of stably optimizing each individual value (Section 5). We present pseudocode for latent quantization and computing the quantization and commitment losses in Algorithm 1, for training a quantized-latent autoencoder (QLAE) in Algorithm 2 (Appendix A), and for training a quantized-latent InfoWGAN-GP [12, 1, 22] in Algorithm 3 (Appendix A).

---

**Algorithm 1** Latent quantization and computation of codebook losses.

---

```

1: function LatentQuantization(datapoint  $x$ , encoder  $\hat{g}^{-1}$ , discrete value array  $V$ )
2:    $z_c \leftarrow \hat{g}^{-1}(x)$ 
3:    $z \leftarrow \arg \min_{v \in Z} \|z_c - v\|_1, \quad v_j \in V_j, \quad \prod_{j=1}^{n_z} V_j = V$  ▷ implement via (4)
4:    $\mathcal{L}_{\text{quantize}} \leftarrow \|\text{StopGradient}(z_c) - z\|_2^2$  ▷ from VQ-VAE [51]
5:    $\mathcal{L}_{\text{commit}} \leftarrow \|z_c - \text{StopGradient}(z)\|_2^2$  ▷ ibid.
6:    $z \leftarrow z_c + \text{StopGradient}(z - z_c)$  ▷ straight-through gradient estimator [5]
7:   return  $z, \mathcal{L}_{\text{quantize}}, \mathcal{L}_{\text{commit}}$ 

```

---

## 4 InfoMEC: Information-Theoretic Metrics for Disentanglement

To empirically assess latent quantization, we require reliable measures of disentanglement. Here, we provide a unifying account of and improve upon metrics for three key disentanglement properties: modularity, explicitness, and compactness, taking inspiration from several prior works [53, 17, 11, 41, 65, 10]. We take particular care in accounting for design decisions, and while we do not expect this to be the final word on disentanglement metrics, we hope our presentation enables others to clearly understand the decision-making underlying our proposed metrics, InfoMEC, and propose further improvements.

### 4.1 Modularity and Compactness

When  $n_z = n_s$ , ICA asks for the latents to recover the sources up to a permutation and dimension-wise invertible transformation. Due to the dimension-wise transformation, simple measures of success (e.g. correlation) may fail. In contrast, the mutual information between individual sources and latents,

$$I(\mathbf{s}_i; \mathbf{z}_j) := D_{\text{KL}}(p(\mathbf{s}_i, \mathbf{z}_j) \parallel p(\mathbf{s}_i)p(\mathbf{z}_j)), \quad (6)$$

accounts for arbitrary nonlinear dependence between its two arguments. When both are discrete, estimating the mutual information is simple via the empirical joint distribution, but if either is continuous, estimation becomes non-trivial. One can bin a continuous variable and pretend it is discrete [42, 10], but this is sensitive to the binning strategy (e.g., substantial overestimation with coarse binning; see Figure 2 of Ross [55]). A better solution from the mutual information estimation literature is to use the  $k$ -nearest neighbor based KSG estimator [37] which has seen widespread use [18]. While this estimator originated for continuous-continuous variables, a variant of KSG [55] also exists for the discrete-continuous case. This is what we use for evaluating models with continuous latents as the datasets used in this work have discrete sources. We use  $k = 3$  to remain in the low-bias regime [18, 37]. We remark that latent quantization, however, permits reliable evaluation using the simpler discrete-discrete estimator.

To normalize mutual information to the interval  $[0, 1]$  (to facilitate aggregation and comparison), we make use of the identity  $I(\mathbf{s}_i; \mathbf{z}_j) = H(\mathbf{s}_i) - H(\mathbf{s}_i | \mathbf{z}_j)$  and the fact that a discrete source’s entropy is nonnegative, so  $I(\mathbf{s}_i; \mathbf{z}_j)$  is bounded above by  $H(\mathbf{s}_i)$ . Following [11], we define a normalized mutual information as

$$\text{NMI}(\mathbf{s}_i, \mathbf{z}_j) := \frac{I(\mathbf{s}_i; \mathbf{z}_j)}{H(\mathbf{s}_i)}. \quad (7)$$

We prefer this normalization scheme over others [60] since i) it is the proportion of entropy in a source reduced by conditioning on a latent, and thus scales consistently to  $[0, 1]$  for any model, and ii) only normalizing by the marginal source entropy avoids the scale-dependent (and possibly negative) marginal differential entropy of a continuous latent, which is itself non-trivial to estimate [37]. We gather all  $n_s \times n_z$  evaluations of  $\text{NMI}(\mathbf{s}_i, \mathbf{z}_j)$  into a 2-dimensional array  $\text{NMI} \in [0, 1]^{n_s \times n_z}$ . We remove columns of NMI corresponding to inactive latents, which we define heuristically as those whose range over the evaluation sample is less than  $1/8$  of that of the latent with largest range.

**Modularity** is the extent to which sources are separated into disjoint sets of latents. Perfect modularity is when every latent is informative of only one source, i.e. when every column of NMI has only one

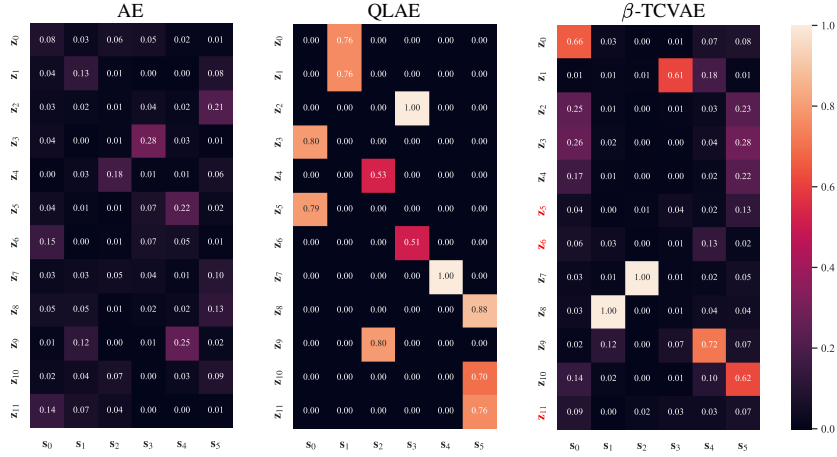


Figure 3: Visualization of  $\text{NMI}^\top$  for models trained on the Shapes3D dataset. Latents in red font are inactive and hence removed from InfoM and InfoC computation. The low values in the  $\text{NMI}^\top$  of AE indicate that individual latents are not highly informative of individual sources. Adding latent quantization results in QLAE achieving near-perfect InfoM (0.99): each latent is only informative of one source (rows are sparse). This induces a trade-off with InfoC, in which  $\beta$ -TCVAE scores higher (0.53 vs. 0.62).

nonzero element (after removal of inactive latents). This has been measured as either the *gap* between the two largest entries in a column [11], or the *ratio* of the largest entry in the column to the column sum [65]. We prefer the ratio since the gap is agnostic to the smallest  $n_s - 2$  values in the column, but how close these values are to 0 matters and should be reflected in the measure. Since the possible range of values for this ratio is  $[1/n_s, 1]$ , we re-normalize to  $[0, 1]$ . Finally, we define modularity as the average of this quantity over latents:

$$\text{InfoM} := \left( \frac{1}{n_z} \sum_{j=1}^{n_z} \frac{\max_i \text{NMI}_{ij}}{\sum_{i=1}^{n_s} \text{NMI}_{ij}} - \frac{1}{n_s} \right) / \left( 1 - \frac{1}{n_s} \right). \quad (8)$$

**Compactness** complements modularity; it is the extent to which latents only contain information about disjoint sets of sources. We therefore define it analogously to modularity, but considering rows of NMI instead of columns, and averaging over sources instead of latents, etc.:

$$\text{InfoC} := \left( \frac{1}{n_s} \sum_{i=1}^{n_s} \frac{\max_j \text{NMI}_{ij}}{\sum_{j=1}^{n_z} \text{NMI}_{ij}} - \frac{1}{n_z} \right) / \left( 1 - \frac{1}{n_z} \right). \quad (9)$$

We advocate for this terminology since previous names such as “mutual information gap” [11] and “mutual information ratio” [65] are ambiguous, and indeed the former of these works considered solely compactness and the latter solely modularity, with neither mentioning the distinction. We remark that when  $n_z > n_s$  (after pruning inactive latents), it is impossible to achieve both perfect modularity and perfect compactness. Of the two, modularity should be prioritized [53, 10] and indeed has been referred to as disentanglement itself [17].

## 4.2 Explicitness

Modularity and compactness are measured in terms of mutual information, so they are agnostic to *how* this information is encoded. Our third metric, explicitness, measures the extent to which the relationship between the sources and latents is simple (e.g., linear [17, 54]). Since previous explicitness metrics have been fairly ad hoc, we suggest a formalism using the framework of predictive  $\mathcal{V}$ -information, a generalization of mutual information that specifies an allowable function class, denoted  $\mathcal{V}$ , for the computation of information. Our presentation of predictive  $\mathcal{V}$ -information is informal; for technical precision readers are encouraged to read Xu et al. [68]. We first estimate the predictive  $\mathcal{V}$ -information of each source  $s_i$  given *all* latents  $\mathbf{z}$ :

$$I_{\mathcal{V}}(\mathbf{z} \rightarrow s_i) = H_{\mathcal{V}}(s_i | \emptyset) - H_{\mathcal{V}}(s_i | \mathbf{z}). \quad (10)$$

This requires estimating the predictive conditional  $\mathcal{V}$ -entropy

$$H_{\mathcal{V}}(s_i | \mathbf{z}) = \inf_{f \in \mathcal{V}} \mathbb{E}_{s \sim p(\mathbf{s}), z \sim p(\mathbf{z}|\mathbf{s})} [-\log p(s_i | f(\mathbf{z}))] \quad (11)$$

and the marginal  $\mathcal{V}$ -entropy of the source

$$H_{\mathcal{V}}(\mathbf{s}_i | \emptyset) = \inf_{f \in \mathcal{V}} \mathbb{E}_{s \sim p(\mathbf{s})} [-\log p(s_i | f(\emptyset))], \quad (12)$$

where  $\emptyset$  is an uninformative constant. The predictive conditional  $\mathcal{V}$ -entropy measures how well a source,  $s_i$ , can be predicted by mapping the latents,  $\mathbf{z}$ , through a function in function class  $\mathcal{V}$ . We note this estimation uses the best *in-sample* negative log likelihood, rather than *out-of-sample* (generalisation) as in machine learning. We choose  $\mathcal{V}$  to be the space of linear models (though one could pick  $\mathcal{V}$  to fit particular needs) and so use logistic regression (linear regression) for discrete (continuous) sources. We use no regularization. We compute the marginal  $\mathcal{V}$ -entropy  $H_{\mathcal{V}}(\mathbf{s}_i | \emptyset)$  in the same way, but substituting a universal constant for all inputs. We propose a simple normalization analogous to the one done for modularity and compactness:

$$\text{NMI}_{\mathcal{V}}(\mathbf{z} \rightarrow \mathbf{s}_i) := \frac{I_{\mathcal{V}}(\mathbf{z} \rightarrow \mathbf{s}_i)}{H_{\mathcal{V}}(\mathbf{s}_i | \emptyset)}, \quad (13)$$

which can be interpreted as the relative reduction in the  $\mathcal{V}$ -entropy of a source achieved by knowing the latents, and is in  $[0, 1]$ : for discrete variables negative log likelihood is the cross-entropy, and for regression we leverage Propositions 1.3 and 1.5 from Xu et al. [68] to argue that  $\text{NMI}_{\mathcal{V}}(\mathbf{z} \rightarrow \mathbf{s}_i) = R^2$ , the coefficient of determination. We can now compute explicitness as:

$$\text{InfoE} := \frac{1}{n_s} \sum_{i=1}^{n_s} \text{NMI}_{\mathcal{V}}(\mathbf{z} \rightarrow \mathbf{s}_i). \quad (14)$$

In summary, we have derived three metrics for evaluating the modularity, explicitness, and compactness of a representation. Each metric has a straightforward information-theoretic interpretation and all share a range of  $[0, 1]$ . We order them in decreasing importance and collectively refer to them as InfoMEC := (InfoM, InfoE, InfoC).

## 5 Experiments

Our experiments aim to answer the following questions: Does latent quantization improve disentanglement? How does it compare against the strongest known methods that operate under the same assumptions? And finally, which of our design choices were critical?

To facilitate this, we benchmark on four established disentanglement datasets: Shapes3D [9], MPI3D [19], Falcor3D [49], and Isaac3D [49]. Dataset details are presented in Appendix B.1. Each consists of RGB image observations generated (near-)noiselessly from all exhaustive combinations of discretely sampled sources. To use a consistent architecture, we downsample the observations to  $64 \times 64$  if necessary. Shapes3D is toyish and useful for rapid prototyping, but the others are chosen for their difficulty [50, 19]. In particular, we use the `complex_shapes` variant of MPI3D collected on a real world robotics apparatus.



Figure 4: Generations from a QLAE trained on the Isaac3D dataset. In each row, a data sample  $x$  is encoded into its latent representation  $\mathbf{z}$ , and  $z_{15}$  is linearly interpolated between its maximum and minimum value across the dataset while all other latent dimensions remain fixed, before being decoded into an image. We observe that  $\mathbf{z}_{15}$  only and wholly encodes background color: only this source varies across columns, and across rows, where only  $z_{15}$  is held constant, color is consistent.

Aside from the baseline AE and InfoGAN methods that we endow with quantized latents, we assemble a modestly sized but representative set of prior methods to compare to:  $\beta$ -VAE [24],  $\beta$ -TCVAE [11], and BioAE [65]. To our knowledge, these are the strongest autoencoder variants for disentanglement that do not bring in additional complexity or additional problem assumptions. In fact, latent quantization would be compatible with many of the ideas in the literature, so instead we focus on a fair empirical comparison of our method with simple but competitive prior methods.

The choice of decoder architecture is known to impose inductive biases relevant for disentanglement [31, 39]. We ensure fair comparison by using the same architecture based on StyleGAN [31, 50] for all methods (Appendix B.3). We follow prior work [42] in considering a statistical learning problem rather than a machine learning one: we train on the entire dataset then evaluate on 10,000 i.i.d. samples. We fix the number of latents in each method to twice the number of sources and tune one key regularization hyperparameter per method per dataset with a thorough sweep (Table 11, Appendix B.2). We use the best performing configurations over 2 seeds and rerun with 5 more seeds. Despite our modest list of methods and ablations, just the last stage took over 1000 GPU-hours.

Table 1: Summary of disentanglement results. Modularity is the key property, followed by (linear) explicitness, with compactness a distant third (grayed). AE and InfoGAN variants are presented and bolded separately as all AEs are filtered for near-perfect data reconstruction, whereas InfoGANs are generally more lossy. For confidence intervals and data reconstruction results, see Appendix C.

model	InfoMEC := (InfoM InfoE InfoC) $\uparrow$														
	aggregated			Shapes3D			MPI3D			Falcor3D		Isaac3D			
AE	(0.37	<b>0.82</b>	0.18)	(0.36	<b>1.00</b>	0.12)	(0.33	<b>0.70</b>	0.17)	(0.37	<b>0.76</b>	0.26)	(0.41	0.81	0.15)
$\beta$ -VAE	(0.58	<b>0.83</b>	0.57)	(0.53	<b>1.00</b>	0.48)	(0.45	<b>0.71</b>	0.50)	<b>(0.70</b>	<b>0.76</b>	0.70)	(0.65	<b>0.84</b>	0.61)
$\beta$ -TCVAE	(0.59	0.66	0.59)	(0.61	0.82	0.62)	<b>(0.53</b>	0.54	0.59)	(0.59	<b>0.71</b>	0.54)	(0.64	0.56	0.60)
BioAE	(0.56	0.76	0.34)	(0.56	<b>1.00</b>	0.46)	(0.45	<b>0.68</b>	0.30)	(0.56	<b>0.72</b>	0.26)	(0.67	0.65	0.36)
QLAE (ours)	<b>(0.77</b>	<b>0.84</b>	0.50)	<b>(0.91</b>	<b>1.00</b>	0.53)	<b>(0.62</b>	<b>0.66</b>	0.54)	<b>(0.72</b>	<b>0.77</b>	0.43)	<b>(0.81</b>	<b>0.93</b>	0.51)
InfoWGAN-GP	(0.52	<b>0.52</b>	0.26)	(0.63	<b>0.76</b>	0.40)	(0.45	0.35	0.19)	(0.50	0.44	0.26)	(0.52	<b>0.52</b>	0.20)
QLInfoWGAN-GP (ours)	<b>(0.71</b>	<b>0.62</b>	0.50)	<b>(0.79</b>	<b>0.76</b>	0.51)	<b>(0.65</b>	<b>0.52</b>	0.38)	<b>(0.72</b>	<b>0.56</b>	0.59)	<b>(0.68</b>	<b>0.62</b>	0.53)

**Effect of latent quantization.** Adding latent quantization to AE (making QLAE) and InfoWGAN-GP (making QLInfoWGAN-GP) results in consistent and dramatic increases in modularity with no compromise on explicitness or compactness (Table 1). This is supportive evidence that latent quantization is a good inductive bias for disentanglement (see also Figures 3 and 4).

**Comparison with prior methods.** QLAE achieves a higher modularity than all prior methods on all four datasets considered while maintaining a competitive explicitness in aggregate with AE and  $\beta$ -VAE. In contrast,  $\beta$ -VAE and  $\beta$ -TCVAE fare better in compactness. This was a useful sanity check: the objectives in these methods contain a term that explicitly minimizes the total correlation, aka multiinformation, amongst the latent variables [11], which essentially optimizes for InfoC.

**Ablations on regularization and latent quantization.** We observe that weight decay is critical to the overall performance of QLAE and QLInfoWGAN-GP (Table 2). However, even without weight decay, QLAE still slightly outperforms all prior methods in Table 1. We also observe the benefit of discretization for modularity in the moderately well-performing VQ-VAE w/ weight decay (which ablates the scalar code design choice of QLAE). However, the high-dimensional latent bottleneck of vector quantization necessitates the use of categorical codes when evaluating on disentanglement metrics, severely compromising the explicitness of the representation. Finally, QLAE with a global codebook as opposed to separate per-dimension codebooks suffers a minor but noticeable penalty in performance, supporting the benefit of the latter for optimization described in Section 3.

Table 2: Summary of ablation studies on QLAE and QLInfoWGAN-GP.

model	InfoMEC := (InfoM InfoE InfoC) $\uparrow$														
	aggregated			Shapes3D			MPI3D			Falcor3D		Isaac3D			
QLAE (ours)	<b>(0.77</b>	<b>0.84</b>	0.50)	<b>(0.91</b>	<b>1.00</b>	0.53)	<b>(0.62</b>	<b>0.66</b>	0.54)	<b>(0.72</b>	<b>0.77</b>	0.43)	<b>(0.81</b>	<b>0.93</b>	0.51)
QLAE w/ global codebook	<b>(0.72</b>	<b>0.84</b>	0.42)	<b>(0.93</b>	<b>1.00</b>	0.48)	<b>(0.60</b>	<b>0.76</b>	0.38)	(0.65	<b>0.72</b>	0.33)	(0.72	<b>0.89</b>	0.50)
QLAE w/o weight decay	(0.66	<b>0.83</b>	0.51)	(0.68	0.99	0.55)	<b>(0.54</b>	<b>0.64</b>	0.57)	<b>(0.65</b>	<b>0.77</b>	0.34)	<b>(0.76</b>	<b>0.92</b>	0.58)
VQ-VAE w/ weight decay	(0.66	0.22	0.41)	(0.82	0.29	0.54)	(0.44	0.25	0.39)	<b>(0.71</b>	0.18	0.47)	(0.67	0.15	0.25)
VQ-VAE w/o weight decay	(0.55	0.15	0.40)	(0.70	0.19	0.50)	(0.41	0.21	0.28)	(0.57	0.07	0.38)	(0.52	0.15	0.44)
QLInfoWGAN-GP (ours)	<b>(0.71</b>	<b>0.62</b>	0.50)	<b>(0.79</b>	<b>0.76</b>	0.51)	<b>(0.65</b>	<b>0.52</b>	0.38)	<b>(0.72</b>	<b>0.56</b>	0.59)	<b>(0.68</b>	<b>0.62</b>	0.53)
QLInfoWGAN-GP w/o weight decay	(0.62	<b>0.53</b>	0.51)	(0.63	0.50	0.35)	<b>(0.66</b>	<b>0.56</b>	0.57)	<b>(0.62</b>	<b>0.55</b>	0.59)	(0.56	<b>0.51</b>	0.56)

## 6 Related Work

**Representation learning with discrete representations.** Discrete representations can be a natural design choice for many deep learning problems, but their use was initially limited by optimization difficulties. Vector quantization [51] overcame these problems using straight-through gradient estimation and a well-designed loss function (we adapt both techniques for our purposes). It has since been broadly applied, e.g., to videos [63, 69], audio [2, 15, 62, 6], and anomaly detection [46].

Of particular relevance are works that learn multiple codebooks, or, equivalently, partition the representation so that certain dimensions can only access certain codes. A few methods, like ours, use one scalar codebook per latent dimension, but for efficiency in retrieval [3, 61, 30, 66] rather than for disentanglement. Others project to multiple subspaces which each have their own codebook [45]. Most related in purpose is the work of Kobayashi et al. [36] who use two separate codebooks to disentangle medical images into normal and abnormal features. Their work enforces disentanglement using supervision—each training image comes with a mask that labels the abnormality, and the abnormal codebook is only used to predict this mask. In contrast, our approach uses per-dimension codebooks to disentangle all the sources of variation in a dataset without requiring supervision.

**Nonlinear ICA and disentangled representation learning.** There is a long history of trying to build interpretable representations that tease out the sources of variation in a dataset. This goes back to classic work on (linear) ICA [13, 28], and has been known in deep learning as disentanglement [4]. Without assumptions, nonlinear ICA and its relatives in the disentanglement literature are provably underspecified [29, 42]. One class of methods makes the problem well specified using partial or weak supervision, such as labeling a small number of sources in a dataset [50] or showing pairs of datapoints in which only one or a few sources differ [57, 43]. More in line with our work are approaches that assume additional source structure and disentangle by ensuring the representation reflects this structure [67]. Assumptions and methods include: VAEs with factorized priors [24, 11], biologically inspired activity constraints [65], sparse source variation over time [59, 35], (structurally) sparse source to pixel influence [71, 48], geometric assumptions on the source to image mapping [58, 70, 25, 21], hierarchical decoding [39], sparse underlying causal graphs between sources [38], and piecewise linearity [34]. Our method, latent quantization, is a continuation of this literature’s ongoing search for generally useful inductive biases for disentanglement.

## 7 Discussion

We have proposed to use latent quantization and model regularization to impose a compositional inductive bias that enables networks to outperform strong prior methods across four disentanglement benchmarks and two model classes (autoencoders and InfoGANs). Ablations showed that both components are critical. We also synthesized ideas on evaluation from the literature into InfoMEC, three information-theoretic metrics for disentangled representations that avoid common issues with pre-existing metrics.

While our results are promising, one concern might be that we have overfit our inductive bias to existing disentanglement benchmarks, in which, just like our model, the sources are discrete and the generative process is noiseless. In the future we will test our methods on datasets with continuous source variables and noisy generative processes. Nevertheless, for now we note that while we use only 10 discrete values per latent dimension, some sources in the benchmark datasets take on four times as many discrete values, suggesting our method may scale favorably to continuous sources.

We do not have any formal understanding of why our method performs as well as it does beyond the compositionality and parsimony intuitions we presented. Further work should try to understand this empirically, e.g., by probing how QLAE distributes data around its latent space, and how weight decay changes this. This will allow QLAE to interface with the ongoing theoretical work that aims to understand the assumptions required to successfully disentangle [38, 65, 8, 21, 25, 32, 34, 35, 71, 67].

Lastly, we hope this method, its future versions, and other methods the field develops are able to deliver on the original promise of disentangled representation learning—to learn human-interpretable representations in complex, real-world situations, and to leverage the interpretability to empower human decision-making. This will require methods that can disentangle out-of-distribution data samples, that work for generic data types, and that can learn (or infer) compositional primitives from sparse interactions with data. We are optimistic that latent quantization is a step in the direction towards robust, interpretable, and flexible learning in neural networks.

## Acknowledgments and Disclosure of Funding

We gratefully acknowledge the developers of open-source software packages that facilitated this research: NumPy [23], JAX [7], Equinox [33], matplotlib [27], seaborn [64], and scikit-learn [52]. We also thank Evan Liu and Kaylee Burns for feedback on an early draft.

KH was funded by a Sequoia Capital Stanford Graduate Fellowship. Part of WD’s work on this project happened during a visit to Stanford funded by the Bogue Fellowship. JCRW was funded by a Henry Wellcome Post-doctoral Fellowship (222817/Z/21/Z). This work was also in part supported by the Stanford Institute for Human-Centered AI (HAI), NSF RI #2211258, AFOSR FA9550-23-1-0127, and ONR MURI N00014-22-1-2740.

## References

- [1] Martin Arjovsky, Soumith Chintala, and Léon Bottou. Wasserstein generative adversarial networks. In *International Conference on Machine Learning*, 2017.
- [2] Alexei Baeovski, Steffen Schneider, and Michael Auli. vq-wav2vec: self-supervised learning of discrete speech representations. In *International Conference on Learning Representations*, 2020.
- [3] Johannes Ballé, Valero Laparra, and Eero P. Simoncelli. End-to-end optimized image compression. In *International Conference on Learning Representations*, 2017.
- [4] Yoshua Bengio. Deep learning of representations: looking forward. In *Statistical Language and Speech Processing*, 2013.
- [5] Yoshua Bengio, Nicholas Léonard, and Aaron Courville. Estimating or propagating gradients through stochastic neurons for conditional computation. *arXiv preprint arXiv:1308.3432*, 2013.
- [6] Zalán Borsos, Raphaël Marinier, Damien Vincent, Eugene Kharitonov, Olivier Pietquin, Matt Sharifi, Olivier Teboul, David Grangier, Marco Tagliasacchi, and Neil Zeghidour. AudioLM: a language modeling approach to audio generation. *arXiv preprint arXiv:2209.03143*, 2022.
- [7] James Bradbury, Roy Frostig, Peter Hawkins, Matthew James Johnson, Chris Leary, Dougal Maclaurin, George Necula, Adam Paszke, Jake VanderPlas, Skye Wanderman-Milne, and Qiao Zhang. JAX: composable transformations of Python+NumPy programs, 2018. URL <http://github.com/google/jax>.
- [8] Simon Buchholz, Michel Besserve, and Bernhard Schölkopf. Function classes for identifiable nonlinear independent component analysis. In *Advances in Neural Information Processing Systems*, 2022.
- [9] Chris Burgess and Hyunjik Kim. 3D shapes dataset, 2018. URL <https://github.com/deepmind/3dshapes-dataset/>.
- [10] Marc-André Carbonneau, Julian Zaidi, Jonathan Boilard, and Ghyslain Gagnon. Measuring disentanglement: a review of metrics. *IEEE Transactions on Neural Networks and Learning Systems*, 2022.
- [11] Ricky TQ Chen, Xuechen Li, Roger B Grosse, and David K Duvenaud. Isolating sources of disentanglement in variational autoencoders. In *Advances in Neural Information Processing Systems*, 2018.
- [12] Xi Chen, Yan Duan, Rein Houthoofd, John Schulman, Ilya Sutskever, and Pieter Abbeel. Infogan: interpretable representation learning by information maximizing generative adversarial nets. In *Advances in Neural Information Processing Systems*, 2016.
- [13] Pierre Comon. Independent component analysis, a new concept? *Signal processing*, 36(3): 287–314, 1994.
- [14] Elliot Creager, David Madras, Joern-Henrik Jacobsen, Marissa Weis, Kevin Swersky, Toniann Pitassi, and Richard Zemel. Flexibly fair representation learning by disentanglement. In *International Conference on Machine Learning*, 2019.

- [15] Prafulla Dhariwal, Heewoo Jun, Christine Payne, Jong Wook Kim, Alec Radford, and Ilya Sutskever. Jukebox: a generative model for music. *arXiv preprint arXiv:2005.00341*, 2020.
- [16] Mengnan Du, Ninghao Liu, and Xia Hu. Techniques for interpretable machine learning. *Communications of the ACM*, 63(1):68–77, 2019.
- [17] Cian Eastwood and Christopher KI Williams. A framework for the quantitative evaluation of disentangled representations. In *International Conference on Learning Representations*, 2018.
- [18] Weihao Gao, Sewoong Oh, and Pramod Viswanath. Demystifying fixed  $k$ -nearest neighbor information estimators. *IEEE Transactions on Information Theory*, 64(8):5629–5661, 2018.
- [19] Muhammad Waleed Gondal, Manuel Wuthrich, Djordje Miladinovic, Francesco Locatello, Martin Breidt, Valentin Volchkov, Joel Akpo, Olivier Bachem, Bernhard Schölkopf, and Stefan Bauer. On the transfer of inductive bias from simulation to the real world: a new disentanglement dataset. In *Advances in Neural Information Processing Systems*, 2019.
- [20] Ian Goodfellow, Jean Pouget-Abadie, Mehdi Mirza, Bing Xu, David Warde-Farley, Sherjil Ozair, Aaron Courville, and Yoshua Bengio. Generative adversarial networks. In *Advances in Neural Information Processing Systems*, 2014.
- [21] Luigi Gresele, Julius Von Kügelgen, Vincent Stimper, Bernhard Schölkopf, and Michel Besserve. Independent mechanism analysis, a new concept? In *Advances in Neural Information Processing Systems*, 2021.
- [22] Ishaan Gulrajani, Faruk Ahmed, Martin Arjovsky, Vincent Dumoulin, and Aaron C Courville. Improved training of Wasserstein GANs. In *Advances in Neural Information Processing Systems*, 2017.
- [23] Charles R Harris, K Jarrod Millman, Stéfan J Van Der Walt, Ralf Gommers, Pauli Virtanen, David Cournapeau, Eric Wieser, Julian Taylor, Sebastian Berg, Nathaniel J Smith, et al. Array programming with NumPy. *Nature*, 585(7825):357–362, 2020.
- [24] Irina Higgins, Loic Matthey, Arka Pal, Christopher Burgess, Xavier Glorot, Matthew Botvinick, Shakir Mohamed, and Alexander Lerchner.  $\beta$ -VAE: learning basic visual concepts with a constrained variational framework. In *International Conference on Learning Representations*, 2017.
- [25] Daniella Horan, Eitan Richardson, and Yair Weiss. When is unsupervised disentanglement possible? In *Advances in Neural Information Processing Systems*, 2021.
- [26] Xiaowei Huang, Daniel Kroening, Wenjie Ruan, James Sharp, Youcheng Sun, Emese Thamo, Min Wu, and Xinping Yi. A survey of safety and trustworthiness of deep neural networks: verification, testing, adversarial attack and defence, and interpretability. *Computer Science Review*, 37:100270, 2020.
- [27] John D Hunter. Matplotlib: a 2D graphics environment. *Computing in Science & Engineering*, 9(03):90–95, 2007.
- [28] Aapo Hyvärinen and Erkki Oja. Independent component analysis: algorithms and applications. *Neural Networks*, 13(4-5):411–430, 2000.
- [29] Aapo Hyvärinen and Petteri Pajunen. Nonlinear independent component analysis: existence and uniqueness results. *Neural Networks*, 12(3):429–439, 1999.
- [30] Lukasz Kaiser, Samy Bengio, Aurko Roy, Ashish Vaswani, Niki Parmar, Jakob Uszkoreit, and Noam Shazeer. Fast decoding in sequence models using discrete latent variables. In *International Conference on Machine Learning*, 2018.
- [31] Tero Karras, Samuli Laine, and Timo Aila. A style-based generator architecture for generative adversarial networks. In *Conference on Computer Vision and Pattern Recognition*, 2019.
- [32] Ilyes Khemakhem, Diederik Kingma, Ricardo Monti, and Aapo Hyvarinen. Variational autoencoders and nonlinear ICA: a unifying framework. In *International Conference on Artificial Intelligence and Statistics*, 2020.

- [33] Patrick Kidger and Cristian Garcia. Equinox: neural networks in JAX via callable PyTrees and filtered transformations. *Differentiable Programming Workshop at Neural Information Processing Systems*, 2021.
- [34] Bohdan Kivva, Goutham Rajendran, Pradeep Ravikumar, and Bryon Aragam. Identifiability of deep generative models without auxiliary information. In *Advances in Neural Information Processing Systems*, 2022.
- [35] David A. Klindt, Lukas Schott, Yash Sharma, Ivan Ustyuzhaninov, Wieland Brendel, Matthias Bethge, and Dylan Paiton. Towards nonlinear disentanglement in natural data with temporal sparse coding. In *International Conference on Learning Representations*, 2021.
- [36] Kazuma Kobayashi, Ryuichiro Hataya, Yusuke Kurose, Mototaka Miyake, Masamichi Takahashi, Akiko Nakagawa, Tatsuya Harada, and Ryuji Hamamoto. Decomposing normal and abnormal features of medical images for content-based image retrieval of glioma imaging. *Medical Image Analysis*, 74:102227, 2021.
- [37] Alexander Kraskov, Harald Stögbauer, and Peter Grassberger. Estimating mutual information. *Physical Review E*, 69(6):066138, 2004.
- [38] Sebastien Lachapelle, Pau Rodriguez, Yash Sharma, Katie E Everett, Rémi Le Priol, Alexandre Lacoste, and Simon Lacoste-Julien. Disentanglement via mechanism sparsity regularization: a new principle for nonlinear ICA. In *Conference on Causal Learning and Reasoning*, 2022.
- [39] Felix Leeb, Giulia Lanzillotta, Yashas Annadani, Michel Besserve, Stefan Bauer, and Bernhard Schölkopf. Structure by architecture: structured representations without regularization. In *International Conference on Learning Representations*, 2023.
- [40] Piyawat Lertvittayakumjorn and Francesca Toni. Explanation-based human debugging of NLP models: a survey. *Transactions of the Association for Computational Linguistics*, 9:1508–1528, 2021.
- [41] Zhiyuan Li, Jaideep Vitthal Murkute, Prashna Kumar Gyawali, and Linwei Wang. Progressive learning and disentanglement of hierarchical representations. In *International Conference on Learning Representations*, 2020.
- [42] Francesco Locatello, Stefan Bauer, Mario Lucic, Gunnar Raetsch, Sylvain Gelly, Bernhard Schölkopf, and Olivier Bachem. Challenging common assumptions in the unsupervised learning of disentangled representations. In *International Conference on Machine Learning*, 2019.
- [43] Francesco Locatello, Ben Poole, Gunnar Rätsch, Bernhard Schölkopf, Olivier Bachem, and Michael Tschannen. Weakly-supervised disentanglement without compromises. In *International Conference on Machine Learning*, 2020.
- [44] Ilya Loshchilov and Frank Hutter. Decoupled weight decay regularization. In *International Conference on Learning Representations*, 2019.
- [45] Zepu Lu, Defu Lian, Jin Zhang, Zaixi Zhang, Chao Feng, Hao Wang, and Enhong Chen. Differentiable optimized product quantization and beyond. In *ACM Web Conference*, 2023.
- [46] Sergio Naval Marimont and Giacomo Tarroni. Anomaly detection through latent space restoration using vector quantized variational autoencoders. In *International Symposium on Biomedical Imaging*, 2021.
- [47] Brent Mittelstadt. Auditing for transparency in content personalization systems. *International Journal of Communication*, 10:12, 2016.
- [48] Gemma Elyse Moran, Dhanya Sridhar, Yixin Wang, and David Blei. Identifiable deep generative models via sparse decoding. *Transactions on Machine Learning Research*, 2022.
- [49] Weili Nie. High resolution disentanglement datasets, 2019. URL <https://github.com/NVlabs/High-res-disentanglement-datasets>.

- [50] Weili Nie, Tero Karras, Animesh Garg, Shoubhik Debnath, Anjul Patney, Ankit B Patel, and Anima Anandkumar. Semi-supervised StyleGAN for disentanglement learning. In *International Conference on Machine Learning*, 2020.
- [51] Aäron van den Oord, Oriol Vinyals, and Koray Kavukcuoglu. Neural discrete representation learning. In *Advances in Neural Information Processing Systems*, 2017.
- [52] Fabian Pedregosa, Gaël Varoquaux, Alexandre Gramfort, Vincent Michel, Bertrand Thirion, Olivier Grisel, Mathieu Blondel, Peter Prettenhofer, Ron Weiss, Vincent Dubourg, Jake Vanderplas, Alexandre Passos, David Cournapeau, Matthieu Brucher, Matthieu Perrot, and Édouard Duchesnay. Scikit-learn: machine learning in Python. *Journal of Machine Learning Research*, 12(85):2825–2830, 2011.
- [53] Karl Ridgeway. A survey of inductive biases for factorial representation-learning. *arXiv preprint arXiv:1612.05299*, 2016.
- [54] Karl Ridgeway and Michael C Mozer. Learning deep disentangled embeddings with the F-statistic loss. In *Advances in Neural Information Processing Systems*, 2018.
- [55] Brian C Ross. Mutual information between discrete and continuous data sets. *PLOS ONE*, 9(2): 1–5, 2014.
- [56] Philipp Schmidt and Felix Biessmann. Quantifying interpretability and trust in machine learning systems. In *AAAI Workshop on Network Interpretability for Deep Learning*, 2019.
- [57] Rui Shu, Yining Chen, Abhishek Kumar, Stefano Ermon, and Ben Poole. Weakly supervised disentanglement with guarantees. In *International Conference on Learning Representations*, 2020.
- [58] Peter Sorrenson, Carsten Rother, and Ullrich Köthe. Disentanglement by nonlinear ICA with general incompressible-flow networks (GIN). In *International Conference on Learning Representations*, 2020.
- [59] Henning Sprekeler, Tiziano Zito, and Laurenz Wiskott. An extension of slow feature analysis for nonlinear blind source separation. *Journal of Machine Learning Research*, 15(1):921–947, 2014.
- [60] Alexander Strehl and Joydeep Ghosh. Cluster ensembles—a knowledge reuse framework for combining multiple partitions. *Journal of Machine Learning Research*, 3(Dec):583–617, 2002.
- [61] Lucas Theis, Wenzhe Shi, Andrew Cunningham, and Ferenc Huszár. Lossy image compression with compressive autoencoders. In *International Conference on Learning Representations*, 2017.
- [62] Andros Tjandra, Sakriani Sakti, and Satoshi Nakamura. Transformer VQ-VAE for unsupervised unit discovery and speech synthesis: ZeroSpeech 2020 challenge. In *INTERSPEECH*, 2020.
- [63] Jacob Walker, Ali Razavi, and Aäron van den Oord. Predicting video with VQVAE. *arXiv preprint arXiv:2103.01950*, 2021.
- [64] Michael L Waskom. Seaborn: statistical data visualization. *Journal of Open Source Software*, 6(60):3021, 2021.
- [65] James C R Whittington, Will Dorrell, Surya Ganguli, and Timothy Behrens. Disentanglement with biological constraints: A theory of functional cell types. In *International Conference on Learning Representations*, 2023.
- [66] Hanwei Wu and Markus Flierl. Learning product codebooks using vector-quantized autoencoders for image retrieval. In *Global Conference on Signal and Information Processing*, 2019.
- [67] Quanhan Xi and Benjamin Bloem-Reddy. Indeterminacy in generative models: characterization and strong identifiability. In *International Conference on Artificial Intelligence and Statistics*, 2023.

- [68] Yilun Xu, Shengjia Zhao, Jiaming Song, Russell Stewart, and Stefano Ermon. A theory of usable information under computational constraints. In *International Conference on Learning Representations*, 2020.
- [69] Wilson Yan, Yunzhi Zhang, Pieter Abbeel, and Aravind Srinivas. VideoGPT: video generation using VQ-VAE and transformers. *arXiv preprint arXiv:2104.10157*, 2021.
- [70] Xiaojiang Yang, Yi Wang, Jiacheng Sun, Xing Zhang, Shifeng Zhang, Zhenguo Li, and Junchi Yan. Nonlinear ICA using volume-preserving transformations. In *International Conference on Learning Representations*, 2022.
- [71] Yujia Zheng, Ignavier Ng, and Kun Zhang. On the identifiability of nonlinear ICA: sparsity and beyond. In *Advances in Neural Information Processing Systems*, 2022.

## A Quantized-Latent Models

This section contains pseudocode for QLAE and QLInfoWGAN-GP.

Note that bias parameters in the encoder and decoder are optimized via Adam, not AdamW.

---

**Algorithm 2** Pseudocode for optimizing a quantized-latent autoencoder (QLAE).  
Hyperparameter values are detailed in Appendix B.2.

---

**Require:** dataset  $\mathcal{D}$ , batch size  $b$ , AdamW hyperparameters  $(\alpha, \beta_1, \beta_2, \text{weight decay})$ ,  
loss weights  $\lambda := (\lambda_{\text{reconstruct data}}, \lambda_{\text{quantize}}, \lambda_{\text{commit}})$

- 1: initialize encoder  $\hat{g}^{-1} : \mathcal{X} \rightarrow \mathbb{R}^{n_z}$ , discrete value array  $V \in \mathbb{R}^{n_z \times n_v}$ , decoder  $\hat{g} : \mathbb{R}^{n_z} \rightarrow \mathcal{X}$
- 2: **while**  $(\hat{g}^{-1}, V, \hat{g})$  has not converged **do**
- 3:     **for**  $i = 1, \dots, b$  **do**
- 4:          $x \sim \mathcal{D}$
- 5:          $z, \mathcal{L}_{\text{quantize}}, \mathcal{L}_{\text{commit}} \leftarrow \text{LatentQuantization}(x, \hat{g}^{-1}, V)$  ▷ Algorithm 1
- 6:          $\mathcal{L}_{\text{reconstruct data}} \leftarrow \text{BinaryCrossEntropy}(\hat{g}(z), x)$
- 7:          $\mathcal{L}_{\text{QLAE}}^{(i)} \leftarrow \lambda \cdot (\mathcal{L}_{\text{reconstruct data}}, \mathcal{L}_{\text{quantize}}, \mathcal{L}_{\text{commit}})$
- 8:      $(\hat{g}^{-1}, \hat{g}) \leftarrow \text{AdamW}(\nabla_{(\hat{g}^{-1}, \hat{g})} \frac{1}{b} \sum_{i=1}^b \mathcal{L}_{\text{QLAE}}^{(i)}, (\hat{g}^{-1}, \hat{g}), \alpha, \beta_1, \beta_2, \text{weight decay})$
- 9:      $V \leftarrow \text{Adam}(\nabla_V \frac{1}{b} \sum_{i=1}^b \mathcal{L}_{\text{QLAE}}^{(i)}, V, \alpha, \beta_1, \beta_2)$

---



---

**Algorithm 3** Pseudocode for optimizing a quantized-latent InfoWGAN-GP.  
Hyperparameter values are detailed in Appendix B.2.

---

**Require:** dataset  $\mathcal{D}$ , batch size  $b$ , AdamW hyperparameters  $(\alpha, \beta_1, \beta_2, \text{weight decay})$ ,  
encoder-to-generator update ratio  $n_{e:g}$   
loss weights  $\lambda := (\lambda_{\text{reconstruct latent}}, \lambda_{\text{quantize}}, \lambda_{\text{commit}}, \lambda_{\text{value}}, \lambda_{\text{gradient penalty}})$

- 1: initialize encoder  $\hat{g}^{-1} : \mathcal{X} \rightarrow \mathbb{R}^{n_z}$ , discrete value array  $V \in \mathbb{R}^{n_z \times n_v}$ , decoder  $\hat{g} : \mathbb{R}^{n_z} \rightarrow \mathcal{X}$
- 2: initialize critic  $\hat{g}_c^{-1} : \mathcal{X} \rightarrow \mathbb{R}$
- 3: **while**  $\theta := (\hat{g}^{-1}, V, \hat{g}, \hat{g}_c^{-1})$  has not converged **do**
- 4:     **for**  $t = 1, \dots, n_{e:g}$  **do** ▷ encoder and critic updates
- 5:         **for**  $i = 1, \dots, b$  **do**
- 6:              $x_{\text{real}} \sim \mathcal{D}, z_{\text{fake}} \sim Z, \epsilon \sim \text{Uniform}([0, 1])$
- 7:              $x_{\text{fake}} \leftarrow \hat{g}(z_{\text{fake}})$
- 8:              $\mathcal{L}_{\text{value}} \leftarrow \hat{g}_c^{-1}(x_{\text{fake}}) - \hat{g}_c^{-1}(x_{\text{real}})$  ▷ from WGAN [1]
- 9:              $x_{\text{interpolated}} \leftarrow \epsilon x_{\text{real}} + (1 - \epsilon)x_{\text{fake}}$
- 10:              $\mathcal{L}_{\text{gradient penalty}} \leftarrow (\|\nabla_{x_{\text{interpolated}}} \hat{g}_c^{-1}(x_{\text{interpolated}})\|_2 - 1)^2$  ▷ from WGAN-GP [22]
- 11:              $\hat{z}_{\text{fake}}, \mathcal{L}_{\text{quantize}}, \mathcal{L}_{\text{commit}} \leftarrow \text{LatentQuantization}(x_{\text{fake}}, \hat{g}^{-1}, V)$  ▷ Algorithm 1
- 12:              $\mathcal{L}_{\text{reconstruct latent}} \leftarrow \text{MeanSquaredError}(\hat{z}_{\text{fake}}, z_{\text{fake}})$  ▷ from InfoGAN [12]
- 13:              $\mathcal{L}^{(i)} \leftarrow \lambda \cdot (\mathcal{L}_{\text{reconstruct latent}}, \mathcal{L}_{\text{quantize}}, \mathcal{L}_{\text{commit}}, \mathcal{L}_{\text{value}}, \mathcal{L}_{\text{gradient penalty}})$
- 14:          $(\hat{g}^{-1}, \hat{g}_c^{-1}) \leftarrow \text{AdamW}(\nabla_{(\hat{g}^{-1}, \hat{g}_c^{-1})} \frac{1}{b} \sum_{i=1}^b \mathcal{L}^{(i)}, (\hat{g}^{-1}, \hat{g}_c^{-1}), \alpha, \beta_1, \beta_2, \text{weight decay})$
- 15:     **for**  $i = 1, \dots, b$  **do**
- 16:          $z_{\text{fake}} \sim Z$
- 17:          $x_{\text{fake}} \leftarrow \hat{g}(z_{\text{fake}})$
- 18:          $\mathcal{L}_{\text{value}} \leftarrow -\hat{g}_c^{-1}(x_{\text{fake}})$  ▷ from WGAN [1]
- 19:          $\hat{z}_{\text{fake}}, \mathcal{L}_{\text{quantize}}, \mathcal{L}_{\text{commit}} \leftarrow \text{LatentQuantization}(x_{\text{fake}}, \hat{g}^{-1}, V)$  ▷ Algorithm 1
- 20:          $\mathcal{L}_{\text{reconstruct latent}} \leftarrow \text{MeanSquaredError}(\hat{z}_{\text{fake}}, z_{\text{fake}})$  ▷ from InfoGAN [12]
- 21:          $\mathcal{L}^{(i)} \leftarrow \lambda \cdot (\mathcal{L}_{\text{reconstruct latent}}, \mathcal{L}_{\text{quantize}}, \mathcal{L}_{\text{commit}}, \mathcal{L}_{\text{value}}, 0)$
- 22:      $\hat{g} \leftarrow \text{AdamW}(\nabla_{\hat{g}} \frac{1}{b} \sum_{i=1}^b \mathcal{L}^{(i)}, \hat{g}, \alpha, \beta_1, \beta_2, \text{weight decay})$
- 23:      $V \leftarrow \text{Adam}(\nabla_V \frac{1}{b} \sum_{i=1}^b \mathcal{L}^{(i)}, V, \alpha, \beta_1, \beta_2)$

---

## B Experiment Details

This section contains details on the experiments conducted in this work.

### B.1 Datasets

Table 3: Summary of datasets used for empirical evaluation.

dataset	$n_s$	$ \mathcal{D} $	description
Shapes3D [9]	6	480,000	geometric shapes in a scene with simplistic textures
MPI3D [19]	7	460,800	real robot arm holding objects in a variety of configurations
Falcor3D [49]	7	233,280	single scene illuminated and viewed in varying conditions
Isaac3D [49]	9	737,280	synthetic robot arm holding objects in a variety of configurations

Table 4: Shapes3D sources.

index	description	values
0	floor hue	10
1	object hue	10
2	camera orientation	10
3	object scale	8
4	object shape	4
5	wall hue	15

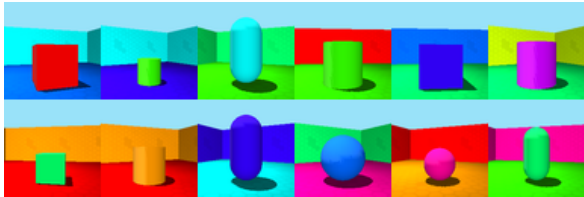


Figure 5: Randomly sampled Shapes3D data.

Table 5: MPI3D sources.

index	description	values
0	object color	4
1	object shape	4
2	object size	2
3	camera height	3
4	background color	3
5	horizontal arm position	40
6	vertical arm position	40

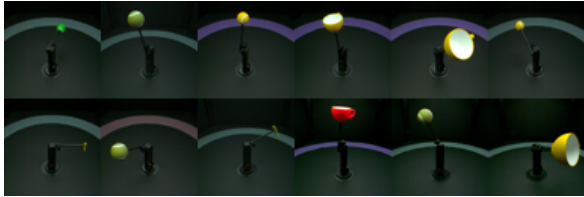


Figure 6: Randomly sampled MPI3D data.

Table 6: Falcor3D sources.

index	description	values
0	lighting intensity	5
1	lighting $x$ position	6
2	lighting $y$ position	6
3	lighting $z$ position	6
4	camera $x$ position	6
5	camera $y$ position	6
6	camera $z$ position	6



Figure 7: Randomly sampled Falcor3D data.

Table 7: Isaac3D sources.

index	description	values
0	object shape	3
1	arm $x$ position	8
2	arm $y$ position	5
3	camera height	4
4	object scale	4
5	lighting intensity	4
6	lighting direction	6
7	object color	4
8	wall color	4



Figure 8: Randomly sampled Isaac3D data.

## B.2 Hyperparameters

This section specifies fixed and tuned hyperparameters for all methods considered.

Table 8: Fixed latent quantization hyperparameters for QLAE and QLInfoWGAN-GP.

hyperparameter	value
$n_v$	10
$V_j$ initialization	$\text{linspace}(-0.5, 0.5, n_v)$
$\lambda_{\text{quantize}}$	$1 \times 10^{-2}$
$\lambda_{\text{commit}}$	$1 \times 10^{-2}$

Table 9: Fixed hyperparameters for all autoencoder variants.

hyperparameter	value
$n_z$	$2n_s$
AdamW learning rate	$1 \times 10^{-3}$
AdamW $\beta_1$	0.9
AdamW $\beta_2$	0.99
AdamW updates	$\leq 2 \times 10^5$
batch size	128
$\lambda_{\text{reconstruct data}}$	1

Table 10: Fixed hyperparameters for all InfoGAN variants.

hyperparameter	value
$n_z$	$2n_s$
AdamW learning rate	$2 \times 10^{-4}$
AdamW $\beta_1$	0
AdamW $\beta_2$	0.9
AdamW updates	$\leq 2 \times 10^5$
batch size	64
$\lambda_{\text{reconstruct latent}}$	200
$\lambda_{\text{gradient penalty}}$	10
$\lambda_{\text{value}}$	1

Table 11: Key regularization hyperparameter tuning done for each autoencoder and InfoGAN variant.

method	hyperparameter	values
AE	weight decay	[0, 0.001, 0.01, 0.1]
BioAE [65]	$\lambda_{\text{activity}}$	[0.01, 0.1, 1, 10, 100]
$\beta$ -VAE [24]	$\beta = \lambda_{\text{KL}}$	[0.1, 0.3, 1, 3, 10]
$\beta$ -TCVAE [11]	$\beta = \lambda_{\text{total correlation}}$	[0.1, 0.3, 1, 3, 10]
VQ-VAE [51] w/ weight decay	weight decay	[0.001, 0.01, 0.1, 1]
QLAE (ours)	weight decay	[0.001, 0.01, 0.1, 1]
InfoWGAN-GP [50]	weight decay	[0.0001, 0.001, 0.01, 0.1]
QLInfoWGAN-GP (ours)	weight decay	[0.0001, 0.001, 0.01, 0.1]

### B.3 Network Architectures

**Encoder.** We use a simple feedforward convolutional encoder network. Each convolutional block consists of two resolution-preserving convolutional layers (kernel size 3, stride 1) and one downsampling convolutional layer (kernel size 4, stride 2) at a consistent width (number of channels). Each convolution operation is followed by a leaky ReLU (slope 0.3), then instance normalization. There are four such blocks with widths 32, 64, 128, and 256. The  $256 \times 4 \times 4$  output is then flattened. Two dense layers each of width 256 with ReLU activation (and no normalization) follow. The final operation is an affine projection to the latent layer.

**Decoder.** We use an architecture based on StyleGAN [31]. The latent code  $z$  of shape  $n_z$  passes through two dense layers each of width 256 with ReLU activation (and no normalization); call the output of this  $w$ . We directly parameterize a starting input feature map of shape  $256 \times 4 \times 4$  with all entries initialized to 0.1. Each style-decoding layer consists of processing an input feature map via a transposed convolution followed by a leaky ReLU (slope 0.3) and then an adaptive instance normalization (AdaIN):  $w$  undergoes an affine projection to a scale and bias scalar for each channel of the output feature map, and the output feature map is instance normalized then affinely transformed by the scales and biases per channel. Similar to the encoder, style-decoding layers are grouped into blocks, with each block consisting of two resolution-preserving style-decoding layers (kernel size 3, stride 1) and one upsampling style-decoding layer (kernel size 4, stride 2) at a consistent width. There are four such blocks with widths 256, 128, 64, and 32. The final operation is a  $1 \times 1$  convolution of width 3 to yield an output of shape  $3 \times 64 \times 64$ .

### B.4 Negative Results

We tried a number of additional modifications to our basic methods, QLAE and QLInfoWGAN-GP, beyond the ablations presented in the main paper. Here is a list of those that only marginally helped, didn't help, or made things worse:

- Keeping the original VQ-VAE [51] hyperparameter settings for  $\lambda_{\text{quantize}}$  (1) and  $\lambda_{\text{commit}}$  (0.25).
- A step function schedule for the weight decay in AdamW: 0 for the first half of optimization, and a specified value for the second half.
- Linearly annealing  $\lambda_{\text{quantize}}$  and/or  $\lambda_{\text{commit}}$  from 0 up to a specified value.
- Using  $\ell_1$  norm parameter vector regularization, in addition to or without weight decay.
- (QLInfoWGAN-GP-specific) Updating V with the encoder instead of with the decoder.

## C Results

This section contains unabridged results for the experiments in the main text. Intervals denote 95% confidence intervals of the mean estimated assuming a  $t$ -distribution. Bolded intervals overlap with the interval with highest endpoint. AE and InfoGAN variants are presented and bolded separately as all AEs are filtered for near-perfect data reconstruction, whereas InfoGANs are generally more lossy.

Table 12: Results aggregated over all datasets.

model	InfoM $\uparrow$	InfoE $\uparrow$	InfoC $\uparrow$	PSNR (dB) $\uparrow$
AE	0.37 $\pm$ 0.03	<b>0.82 <math>\pm</math> 0.03</b>	0.2 $\pm$ 0.1	<b>35.9 <math>\pm</math> 0.5</b>
$\beta$ -VAE	0.58 $\pm$ 0.03	<b>0.83 <math>\pm</math> 0.04</b>	<b>0.57 <math>\pm</math> 0.04</b>	<b>35.1 <math>\pm</math> 0.8</b>
$\beta$ -TCVAE	0.59 $\pm$ 0.03	0.66 $\pm$ 0.06	<b>0.59 <math>\pm</math> 0.06</b>	34.5 $\pm$ 0.6
BioAE	0.56 $\pm$ 0.04	<b>0.76 <math>\pm</math> 0.02</b>	<b>0.3 <math>\pm</math> 0.1</b>	35.1 $\pm$ 0.4
QLAE (ours)	<b>0.77 <math>\pm</math> 0.03</b>	<b>0.84 <math>\pm</math> 0.04</b>	<b>0.5 <math>\pm</math> 0.1</b>	<b>35.8 <math>\pm</math> 0.6</b>
QLAE w/ global codebook	<b>0.72 <math>\pm</math> 0.03</b>	<b>0.8 <math>\pm</math> 0.1</b>	<b>0.4 <math>\pm</math> 0.1</b>	<b>36.2 <math>\pm</math> 0.4</b>
QLAE w/o weight decay	0.66 $\pm$ 0.05	<b>0.83 <math>\pm</math> 0.06</b>	<b>0.5 <math>\pm</math> 0.2</b>	<b>36.0 <math>\pm</math> 0.5</b>
VQ-VAE w/ weight decay	0.66 $\pm$ 0.03	0.22 $\pm$ 0.08	<b>0.41 <math>\pm</math> 0.07</b>	34.8 $\pm$ 0.6
VQ-VAE w/o weight decay	0.55 $\pm$ 0.08	0.15 $\pm$ 0.09	<b>0.4 <math>\pm</math> 0.1</b>	<b>35.3 <math>\pm</math> 0.5</b>
InfoWGAN-GP	0.52 $\pm$ 0.07	<b>0.52 <math>\pm</math> 0.03</b>	0.3 $\pm$ 0.1	<b>19 <math>\pm</math> 3</b>
QLInfoWGAN-GP (ours)	<b>0.71 <math>\pm</math> 0.04</b>	<b>0.62 <math>\pm</math> 0.07</b>	<b>0.50 <math>\pm</math> 0.08</b>	<b>22 <math>\pm</math> 2</b>
QLInfoWGAN-GP w/o weight decay	0.62 $\pm$ 0.05	<b>0.53 <math>\pm</math> 0.04</b>	<b>0.5 <math>\pm</math> 0.1</b>	<b>22 <math>\pm</math> 2</b>

Table 13: Full results for the Shapes3D dataset.

model	InfoM $\uparrow$	InfoE $\uparrow$	InfoC $\uparrow$	PSNR (dB) $\uparrow$
AE	0.36 $\pm$ 0.03	<b>1 <math>\pm</math> 0</b>	0.1 $\pm$ 0.1	<b>36.8 <math>\pm</math> 0.3</b>
$\beta$ -VAE	0.53 $\pm$ 0.03	<b>1 <math>\pm</math> 0</b>	0.48 $\pm$ 0.03	35.0 $\pm$ 0.7
$\beta$ -TCVAE	0.61 $\pm$ 0.02	0.8 $\pm$ 0.1	<b>0.62 <math>\pm</math> 0.05</b>	35.0 $\pm$ 0.8
BioAE	0.56 $\pm$ 0.02	<b>1 <math>\pm</math> 0</b>	0.46 $\pm$ 0.09	35.1 $\pm$ 0.3
QLAE (ours)	<b>0.91 <math>\pm</math> 0.02</b>	<b>1 <math>\pm</math> 0</b>	<b>0.53 <math>\pm</math> 0.08</b>	<b>35.9 <math>\pm</math> 0.7</b>
QLAE w/ global codebook	<b>0.93 <math>\pm</math> 0.03</b>	<b>1 <math>\pm</math> 0</b>	0.48 $\pm$ 0.07	35.9 $\pm$ 0.3
QLAE w/o weight decay	0.68 $\pm$ 0.04	0.985 $\pm$ 0.009	<b>0.5 <math>\pm</math> 0.1</b>	<b>37.0 <math>\pm</math> 0.3</b>
VQ-VAE w/ weight decay	0.82 $\pm$ 0.03	0.29 $\pm$ 0.01	<b>0.54 <math>\pm</math> 0.07</b>	<b>36.9 <math>\pm</math> 0.5</b>
VQ-VAE w/o weight decay	0.70 $\pm$ 0.07	0.19 $\pm$ 0.01	0.50 $\pm$ 0.08	<b>36.5 <math>\pm</math> 0.4</b>
InfoWGAN-GP	0.63 $\pm$ 0.09	<b>0.76 <math>\pm</math> 0.06</b>	<b>0.4 <math>\pm</math> 0.1</b>	13 $\pm$ 2
QLInfoWGAN-GP (ours)	<b>0.79 <math>\pm</math> 0.04</b>	<b>0.76 <math>\pm</math> 0.05</b>	<b>0.51 <math>\pm</math> 0.09</b>	<b>20 <math>\pm</math> 1</b>
QLInfoWGAN-GP w/o weight decay	0.63 $\pm$ 0.06	0.50 $\pm$ 0.05	<b>0.3 <math>\pm</math> 0.1</b>	<b>21 <math>\pm</math> 2</b>

Table 14: Full results for the MPI3D dataset.

model	InfoM $\uparrow$	InfoE $\uparrow$	InfoC $\uparrow$	PSNR (dB) $\uparrow$
AE	0.33 $\pm$ 0.05	<b>0.70 <math>\pm</math> 0.04</b>	0.17 $\pm$ 0.09	<b>39.0 <math>\pm</math> 0.7</b>
$\beta$ -VAE	0.45 $\pm$ 0.04	<b>0.71 <math>\pm</math> 0.03</b>	<b>0.50 <math>\pm</math> 0.05</b>	<b>38.7 <math>\pm</math> 0.7</b>
$\beta$ -TCVAE	<b>0.53 <math>\pm</math> 0.05</b>	<b>0.54 <math>\pm</math> 0.07</b>	<b>0.59 <math>\pm</math> 0.07</b>	35.8 $\pm$ 0.5
BioAE	0.45 $\pm$ 0.02	<b>0.68 <math>\pm</math> 0.03</b>	<b>0.3 <math>\pm</math> 0.1</b>	<b>38.3 <math>\pm</math> 0.6</b>
QLAE (ours)	<b>0.62 <math>\pm</math> 0.06</b>	<b>0.66 <math>\pm</math> 0.05</b>	<b>0.5 <math>\pm</math> 0.1</b>	<b>37.9 <math>\pm</math> 0.9</b>
QLAE w/ global codebook	<b>0.60 <math>\pm</math> 0.04</b>	<b>0.8 <math>\pm</math> 0.2</b>	<b>0.4 <math>\pm</math> 0.1</b>	<b>38.1 <math>\pm</math> 0.4</b>
QLAE w/o weight decay	<b>0.54 <math>\pm</math> 0.06</b>	<b>0.6 <math>\pm</math> 0.1</b>	<b>0.6 <math>\pm</math> 0.2</b>	36.4 $\pm$ 0.8
VQ-VAE w/ weight decay	0.44 $\pm$ 0.03	0.3 $\pm$ 0.1	<b>0.39 <math>\pm</math> 0.04</b>	37 $\pm$ 1
VQ-VAE w/o weight decay	0.41 $\pm$ 0.09	0.2 $\pm$ 0.1	<b>0.3 <math>\pm</math> 0.1</b>	35.5 $\pm$ 0.5
InfoWGAN-GP	0.45 $\pm$ 0.04	0.35 $\pm$ 0.02	0.2 $\pm$ 0.1	<b>25 <math>\pm</math> 2</b>
QLInfoWGAN-GP (ours)	<b>0.65 <math>\pm</math> 0.04</b>	<b>0.52 <math>\pm</math> 0.09</b>	0.38 $\pm$ 0.06	<b>25 <math>\pm</math> 2</b>
QLInfoWGAN-GP w/o weight decay	<b>0.66 <math>\pm</math> 0.04</b>	<b>0.56 <math>\pm</math> 0.04</b>	<b>0.6 <math>\pm</math> 0.1</b>	<b>25 <math>\pm</math> 1</b>

Table 15: Full results for the Falcor3D dataset.

model	InfoM $\uparrow$	InfoE $\uparrow$	InfoC $\uparrow$	PSNR (dB) $\uparrow$
AE	0.37 $\pm$ 0.03	<b>0.76 <math>\pm</math> 0.03</b>	0.3 $\pm$ 0.1	<b>29.9 <math>\pm</math> 0.5</b>
$\beta$ -VAE	<b>0.70 <math>\pm</math> 0.01</b>	<b>0.76 <math>\pm</math> 0.06</b>	<b>0.70 <math>\pm</math> 0.03</b>	28.8 $\pm$ 0.7
$\beta$ -TCVAE	0.59 $\pm$ 0.04	<b>0.71 <math>\pm</math> 0.03</b>	0.54 $\pm$ 0.04	<b>29.3 <math>\pm</math> 0.7</b>
BioAE	0.56 $\pm$ 0.06	<b>0.72 <math>\pm</math> 0.03</b>	0.3 $\pm$ 0.1	<b>29.3 <math>\pm</math> 0.4</b>
QLAE (ours)	<b>0.72 <math>\pm</math> 0.01</b>	<b>0.77 <math>\pm</math> 0.03</b>	0.4 $\pm$ 0.1	<b>29.6 <math>\pm</math> 0.5</b>
QLAE w/ global codebook	0.65 $\pm$ 0.02	<b>0.7 <math>\pm</math> 0.2</b>	0.3 $\pm$ 0.1	<b>30.1 <math>\pm</math> 0.5</b>
QLAE w/o weight decay	<b>0.65 <math>\pm</math> 0.05</b>	<b>0.77 <math>\pm</math> 0.05</b>	0.3 $\pm$ 0.2	<b>29.5 <math>\pm</math> 0.5</b>
VQ-VAE w/ weight decay	<b>0.71 <math>\pm</math> 0.02</b>	0.18 $\pm$ 0.08	0.47 $\pm$ 0.08	29.1 $\pm$ 0.3
VQ-VAE w/o weight decay	0.57 $\pm$ 0.07	0.07 $\pm$ 0.09	0.38 $\pm$ 0.08	<b>29.4 <math>\pm</math> 0.5</b>
InfoWGAN-GP	0.50 $\pm$ 0.05	0.44 $\pm$ 0.03	0.3 $\pm$ 0.1	<b>17 <math>\pm</math> 2</b>
QLInfoWGAN-GP (ours)	<b>0.72 <math>\pm</math> 0.03</b>	<b>0.56 <math>\pm</math> 0.08</b>	<b>0.59 <math>\pm</math> 0.06</b>	<b>17 <math>\pm</math> 3</b>
QLInfoWGAN-GP w/o weight decay	<b>0.62 <math>\pm</math> 0.07</b>	<b>0.55 <math>\pm</math> 0.02</b>	<b>0.59 <math>\pm</math> 0.08</b>	<b>19 <math>\pm</math> 2</b>

Table 16: Full results for the Isaac3D dataset.

model	InfoM $\uparrow$	InfoE $\uparrow$	InfoC $\uparrow$	PSNR (dB) $\uparrow$
AE	0.41 $\pm$ 0.02	<b>0.81 <math>\pm</math> 0.03</b>	0.15 $\pm$ 0.05	38.1 $\pm$ 0.5
$\beta$ -VAE	0.65 $\pm$ 0.02	<b>0.84 <math>\pm</math> 0.07</b>	<b>0.61 <math>\pm</math> 0.03</b>	37.9 $\pm$ 0.9
$\beta$ -TCVAE	0.64 $\pm$ 0.02	0.56 $\pm$ 0.02	<b>0.60 <math>\pm</math> 0.07</b>	38.0 $\pm$ 0.5
BioAE	0.67 $\pm$ 0.05	0.65 $\pm$ 0.04	<b>0.4 <math>\pm</math> 0.1</b>	37.7 $\pm$ 0.5
QLAE (ours)	<b>0.81 <math>\pm</math> 0.02</b>	<b>0.93 <math>\pm</math> 0.06</b>	<b>0.51 <math>\pm</math> 0.08</b>	39.9 $\pm$ 0.2
QLAE w/ global codebook	0.72 $\pm$ 0.03	<b>0.9 <math>\pm</math> 0.1</b>	<b>0.5 <math>\pm</math> 0.1</b>	40.5 $\pm$ 0.1
QLAE w/o weight decay	<b>0.76 <math>\pm</math> 0.05</b>	<b>0.92 <math>\pm</math> 0.07</b>	<b>0.6 <math>\pm</math> 0.2</b>	<b>41.2 <math>\pm</math> 0.3</b>
VQ-VAE w/ weight decay	0.67 $\pm$ 0.03	0.2 $\pm$ 0.1	0.25 $\pm$ 0.08	36.4 $\pm$ 0.4
VQ-VAE w/o weight decay	0.52 $\pm$ 0.07	0.15 $\pm$ 0.09	<b>0.4 <math>\pm</math> 0.1</b>	39.9 $\pm$ 0.5
InfoWGAN-GP	0.52 $\pm$ 0.09	<b>0.52 <math>\pm</math> 0.03</b>	0.20 $\pm$ 0.04	<b>22 <math>\pm</math> 4</b>
QLInfoWGAN-GP (ours)	<b>0.68 <math>\pm</math> 0.04</b>	<b>0.62 <math>\pm</math> 0.07</b>	<b>0.5 <math>\pm</math> 0.1</b>	<b>25 <math>\pm</math> 1</b>
QLInfoWGAN-GP w/o weight decay	0.56 $\pm$ 0.02	<b>0.51 <math>\pm</math> 0.04</b>	<b>0.6 <math>\pm</math> 0.1</b>	<b>25 <math>\pm</math> 1</b>